The structure of LsrB from *Yersinia pestis* complexed with autoinducer-2

Jeffrey S. Kavanaugh,[a] Lokesh Gakhar[b] and Alexander R. Horswill[a]*

[a]Microbiology Department, Roy J. and Lucille A. Carver College of Medicine, University of Iowa, Iowa City, IA 52242, USA, and [b]Protein Crystallography Facility, Roy J. and Lucille A. Carver College of Medicine, University of Iowa, Iowa City, IA 52242, USA

Correspondence e-mail: alex-horswill@uiowa.edu

The crystal structure of LsrB from *Yersinia pestis* complexed with autoinducer-2 (AI-2; space group $P2_12_12_1$, unit-cell parameters $a = 40.61$, $b = 61.03$, $c = 125.23$ Å) has been solved by molecular replacement using the structure of LsrB from *Salmonella typhimurium* (PDB entry 1tjy) and refined to $R = 0.180$ ($R_{\text{free}} = 0.213$) at 1.75 Å resolution. The electron density for bound AI-2 and the stereochemistry of the AI-2-binding site are consistent with bound AI-2 adopting the (2*R*,4*S*)-2-methyl-2,3,3,4-tetrahydroxytetrahydrofuran conformation, just as has been observed in the crystal structures of the *Salmonella typhimurium* and *Sinorhizobium meliloti* LsrB–AI-2 complexes.

1. Introduction

Bacteria can adapt to changes in local population densities by sensing the extracellular concentration of communication signals. This regulatory mechanism is generally called 'quorum sensing' and the types of signals recognized are composed of diverse functional chemistry, ranging from acylhomoserine lactones in Gram-negative species to linear or modified peptides in Gram-positive species (Fuqua *et al.*, 2001; Thoendel & Horswill, 2010). An additional molecule called autoinducer-2 (AI-2) is produced by many species spanning different phylogenetic groups and has been proposed to function as a universal quorum-sensing signal (Surette *et al.*, 1999).

AI-2 was originally identified and characterized in the marine bacterium *Vibrio harveyi* (Bassler *et al.*, 1993). The signal is released into the extracellular environment and induces bioluminescence in a concentration-dependent manner through a two-component sensory relay (Vendeville *et al.*, 2005). The structure of AI-2 was unknown until crystallographic studies of the LuxP periplasmic receptor revealed a bound furanosyl borate diester (2-methyl-2,3,3,4-tetra-hydroxytetrahydrofuran–borate; *S*-THMF–borate) in the active site (Chen *et al.*, 2002). Interestingly, the LuxP receptor and other *V. harveyi* sensory components are not present in many species of bacteria (Sun *et al.*, 2004). Studies on *Salmonella typhimurium* were the first to unravel these differences and to identify the alterative *luxS*-regulated (Lsr) chromosomal locus. Unlike the *V. harveyi* paradigm model, the AI-2 signal is imported into the *S. typhimurium* cytoplasm through the action of an ABC transporter encoded in the *lsr* region (Taga *et al.*, 2001, 2003). The *S. typhimurium* AI-2 structure is also divergent, which was revealed through crystallographic studies of the LsrB periplasmic receptor. The *S. typhimurium* version of AI-2 is a (2*R*,4*S*)-2-methyl-2,3,3,4-tetrahydroxytetrahydrofuran (*R*-THMF) that lacks the liganded B atom (Miller *et al.*, 2004). Subsequent studies demonstrated that both *S*-THMF–borate and *R*-THMF are derived from the common intermediate dihydroxypentanedione (DPD). DPD is produced through the activated methyl cycle, in which *S*-adenosylhomocysteine is converted in sequential steps to
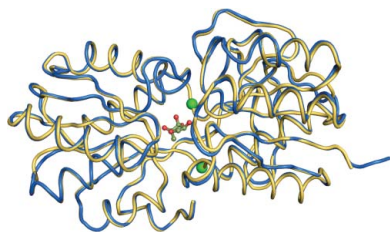
homocysteine and DPD through the action of the Pfs nucleosidase and LuxS enzymes (Miller *et al.*, 2004). More recently, AI-2 in the crystal structure of LsrB–AI-2 from *Sinorhizobium meliloti* (Pereira *et al.*, 2008; PDB entry 3ejw) has been shown to adopt the same *R*-THMF conformation.

Here, we report the LsrB–AI-2 structure for the pathogen *Yersinia pestis*, the causative agent of plague in humans. *Y. pestis* is known to have a *luxS* gene and preliminary studies indicate that it produces AI-2 (Bobrov *et al.*, 2007). We find that AI-2 synthesized from *S*-adenosylhomocysteine using purified Pfs nucleosidase and LuxS enzymes from *Y. pestis* (Yu *et al.*, 2011) adopts the *R*-THMF conformation when bound to *Y. pestis* LsrB.

2. Materials and methods

2.1. Cloning

Avirulent *Y. pestis* CO92 pgm⁻ pCD1 (Lcr⁺, strain R88) was obtained from Robert Perry (University of Kentucky) and maintained in Brain Heart Infusion Broth (BHI). Genomic DNA was purified from strain R88 using a Gentra Puregene bacterial DNA-purification kit (Gentra Systems, Minneapolis, Minnesota, USA) and used as a template source for cloning of *lsrB*. A truncated LsrB lacking the amino-terminal leader sequence (Δ2–25) was PCR-amplified from genomic DNA using the oligonucleotides 5′-GTT-GTTCATATGGCGGAACGCATCGCATTTATC-3′ (forward) and 5′-GTTGTTGGATCCCCGCTAAGATTAAAAGTCGTATTTACT-G-3′ (reverse). The PCR product was digested with *Nde*I and *Bam*HI and cloned into pET28a cut with the same enzymes, resulting in an N-terminal His tag. There is no C-terminal T7 tag owing to the stop codon in the reverse primer. Clones were sequenced at the University of Iowa DNA Core Facility and positive clones were transformed into *Escherichia coli* overexpression strain ER2566 (New England Biolabs).

2.2. Expression and purification

E. coli overexpression strain ER2566 carrying plasmid pET28a-*lsrB* was grown at 310 K in 8 l Luria–Bertani medium to an optical density of ~1.0 at 600 nm. Expression of *lsrB* in the culture was induced with 1 m*M* IPTG for 4 h. The cells were harvested by centrifugation and resuspended in 90 ml equilibration buffer (50 m*M* sodium phosphate pH 8.0, 0.3 *M* sodium chloride, 10 m*M* imidazole). The suspension was lysed with 9 ml Bugbuster (Novagen) and incubated at 277 K with gentle rocking for 4 h. The LsrB protein was purified by nickel-affinity chromatography using His-Select resin (Sigma) by the batch method. After centrifugation at 30 000g for 30 min at 277 K, the cleared lysate was incubated with 25 ml equilibrated resin for 2 h at 277 K with gentle rocking. The resin was then centrifuged at 5000g for 5 min at 277 K and the supernatant was saved. The resin was washed twice with ten volumes of equilibration buffer. The LsrB protein was eluted from the resin with two column volumes of elution buffer (50 m*M* sodium phosphate pH 8.0, 0.3 *M* sodium chloride, 250 m*M* imidazole). Elution fractions were pooled and concentrated using an Amicon PM10 membrane and finally dialyzed against 10 m*M* sodium phosphate pH 6.5. The concentration of His-tagged LsrB was determined to be 22.1 mg ml⁻¹ by the Bradford assay (Bio-Rad).

2.3. Crystallization

Hanging-drop vapor-diffusion crystallization screens were performed using a Mosquito robot (TTP LabTech, Cambridge,

Table 1
Crystal and refinement parameters for LsrB from *Y. pestis* (PDB entry 3t95).

Values in parentheses are for the highest resolution shell.

Data processing	
Wavelength (Å)	1.5418
Unit-cell parameters (Å)	$a = 40.61$, $b = 61.03$, $c = 125.23$
Space group	$P2_12_12_1$
Resolution range (Å)	62.62–1.75 (1.84–1.75)
No. of observations	207868
No. of unique reflections	31947 (4339)
Data completeness (%)	98.9 (93.7)
Multiplicity	6.5 (5.7)
$\langle I/\sigma(I)\rangle$	23.3 (6.5)
R_{merge}	0.049 (0.261)
*REFMAC*5 refinement	
Resolution range (Å)	19.75–1.75 (1.80–1.75)
No. of reflections for R_{work}	30271 (1973)
No. of reflections for R_{free}	1618 (93)
No. of protein atoms	2398
No. of solvent atoms	380
No. of ligand atoms	10
Mean overall B factor (Å^2)	17.4
Mean protein B factor (Å^2)	15.6
Mean solvent B factor (Å^2)	29.3
Mean ligand B factor (Å^2)	9.4
Final R_{work}	0.180 (0.306)
Final R_{free}	0.213 (0.415)
R.m.s.d. bond lengths (Å)	0.013
R.m.s.d. bond angles (°)	1.361
R.m.s.d. B factors (Å^2)	
Main-chain bond-related	0.701
Main-chain angle-related	1.296
Side-chain bond-related	2.168
Side-chain angle-related	3.614

Massachusetts, USA) and pre-filled crystallization trays that were prepared using a Genesis RSP 150/8 liquid handler (Tecan, Männedorf, Switzerland). The drop and reservoir volumes were 0.8 and 100 µl, respectively, with the initial protein concentration in the drops being 11 mg ml⁻¹ (1:1 ratio of protein:well solution). Four different 96-condition screens were utilized: Crystal Screen/Crystal Screen 2 and SaltRx from Hampton Research (Aliso Viejo, California, USA), Wizard I and II from Emerald BioSystems (Bainbridge Island, Washington, USA) and the PEGs and PEGs II Suite from Qiagen (Germantown, Maryland, USA). Crystallization trays were stored at 291 K and the drops were monitored for crystal growth using *RockMaker* software and a RockImager 2 (Formulatrix, Waltham, Massachusetts, USA). Within 2 d, crystals began to form in numerous crystallization conditions, with the most promising crystals growing from drops that had lower molecular-weight PEGs as the precipitating agent. Large (~0.3 × 0.3 × 0.2 mm) well formed single crystals that grew from drops containing 20% PEG 3350 and 200 m*M* diammonium hydrogen phosphate (Qiagen PEGs Suite condition No. 92) were used for data collection after 6 d of growth.

2.4. Diffraction data collection

A single LsrB crystal that was grown from 20% PEG 3350, 200 m*M* diammonium hydrogen phosphate was transferred into 200 µl mother liquor in which the concentration of PEG 3350 was increased to 35%. The mother liquor also contained 145 µ*M* AI-2 that had been synthesized from *S*-adenosylhomocysteine using purified Pfs nucleosidase and LuxS enzymes from *Y. pestis* (Yu *et al.*, 2011). The crystal was soaked at 291 K for approximately 24 h and flash-cooled in a nylon loop for data collection. Diffraction data for the AI-2-soaked crystal were collected at the University of Iowa Protein Crystallography Facility using a Rigaku RUH3R rotating-anode generator that was fitted with Osmic Blue Optics and an R-AXIS IV⁺⁺ area detector (Rigaku, The Woodlands, Texas, USA). The

crystal was maintained at 100 K using an Oxford CryoStream 700. Diffraction data were collected using *StructureStudio* and processed using *XDS* (Kabsch, 2010) and *SCALA* (Evans, 2006) software. Crystal parameters and data-processing statistics are presented in Table 1.

2.5. Structure solution and refinement

The structure of the LsrB–AI-2 complex was solved by molecular replacement using *Phaser* (McCoy *et al.*, 2007) in the *CCP*4 (v.6.1.13) software package (Winn *et al.*, 2011). When the structure of *S. typhimurium* apo LsrB (PDB entry 1tm2; Miller *et al.*, 2004) was used as the probe structure no molecular-replacement solution was obtained, but using the structure of the *S. typhimurium* LsrB–AI2 complex (PDB entry 1tjy; Miller *et al.*, 2004) as a probe did yield a unique molecular-replacement solution. The AI-2 ligand was not included in this probe structure in order to minimize any bias with regard to the molecular form of the AI-2 bound to *Y. pestis* LsrB. Strong well defined electron density was found in the *Y. pestis* LsrB AI-2 binding site, but AI-2 was not added to the atomic model right away. The amino-acid differences (37 positions) between *S. typhimurium* and *Y. pestis* LsrB were incorporated into the model using the *Coot* software package (Emsley *et al.*, 2010) and the model was subjected to maximum-likelihood refinement using *REFMAC*5 (Murshudov *et al.*, 2011). There was interpretable electron density for the entire LsrB sequence (Ala26–Phe339) and some electron density for the last two residues, His24 and Met25, of the N-terminal His tag, but these residues were not added to the atomic model because the weak electron density could not be interpreted unambiguously. A total of 380 water molecules were added to the model in iterations of *Coot* real-space refinement followed by maximum-likelihood refinement using *REFMAC*5. Finally, the AI-2 molecule was added to the model and one round of refinement with *REFMAC*5 resulted in R and R_{free} values of 0.1800 and 0.2128, respectively. The final model

has good stereochemistry, as indicated by the refinement statistics reported in Table 1. The final model and diffraction data have been deposited in the Protein Data Bank (Berman *et al.*, 2000; PDB code 3t95).

3. Results and discussion

3.1. LsrB domain structure

With the similarities of the *Y. pestis lsr* region to those of other enteric bacteria, we hypothesized that *Y. pestis* recognizes the non-boron-containing form of AI-2 (*R*-THMF). To investigate this question, the *Y. pestis* CO92 LsrB protein was overexpressed and purified using nickel-affinity chromatography. The LsrB protein was cocrystallized with AI-2 that had been biosynthesized using recombinant *Y. pestis* LuxS and Pfs proteins. The structure was solved at 1.75 Å resolution by molecular replacement using the structure of the LsrB–AI-2 complex (PDB entry 1tjy) from *S. typhimurium* (Miller *et al.*, 2004).

The LsrBs from *Y. pestis*, *S. typhimurium* and *Si. meliloti* share high sequence similarity (Fig. 1), with the *Y. pestis* sequence being 87% and 76% identical to the *S. typhimurium* and *Si. meliloti* sequences, respectively. All three receptors adopt a class 1 periplasmic binding-protein fold (Quiocho & Ledvina, 1996; Dwyer & Hellinga, 2004), in which two α/β-domains are connected through three short connecting linkers or hinges (Fig. 1) and each α/β-domain is composed of two segments, one coming from the first half of the polypeptide chain and the other from the second half of the chain. The *Y. pestis* LsrB–AI-2 complex shows striking structural similarity to the LsrB–AI-2 complexes from *S. typhimurium* (Miller *et al.*, 2004) and *Si. meliloti* (Pereira *et al.*, 2008), with C$^\alpha$ root-mean-square deviations (r.m.s.d.) of 0.279 Å (269 C$^\alpha$) for *S. typhimurium* and 0.346 Å (267 C$^\alpha$) for chain *A* and 0.271 Å (261 C$^\alpha$) for chain *B* of the *Si. meliloti* asymmetric unit. There is a significant tertiary-structure conformation change asso-
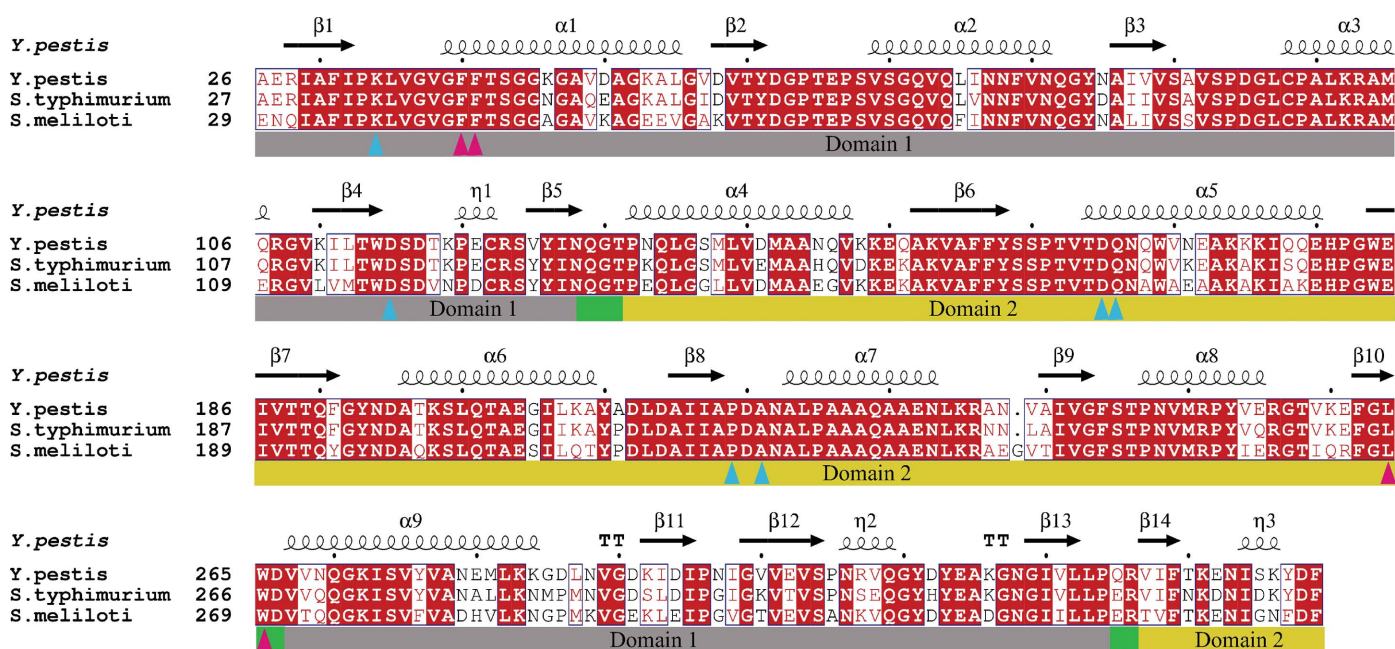

Figure 1
Sequence alignment of LsrB from *Y. pestis*, *S. typhimurium* and *Si. meliloti*, in which residues that are conserved in all three proteins are highlighted with a red background and residues that are conserved in two of the proteins are displayed in red text. Secondary-structural elements of *Y. pestis* LsrB are indicated at the top of each panel. Bars below the sequences indicate domain structure, with hinge residues indicated by green bars and domain 1 and domain 2 residues indicated by grey and yellow bars, respectively. Residues that interact with AI-2 are indicated by triangles: blue for residues that form hydrogen bonds and magenta for residues that form van der Waals interactions. This figure was generated using *ClustalW* (Larkin *et al.*, 2007) and *ESPript/ENDscript* (Gouet *et al.*, 2003).

ciated with binding of AI-2 (Fig. 2), which is evident when one superimposes domain 2 residues Gly130–Asp266 and calculates the r.m.s.d. for the residues that were not superimposed. When the domain 2 residues of the *Y. pestis* LsrB–AI2 complex are super-

Figure 2
Ribbon drawing showing AI-2 bound in the cleft between α/β-domains 1 and 2. (*a*) shows the LsrB–AI-2 complex from *Y. pestis* (yellow) and the LsrB–AI-2 complex from *S. typhimurium* (blue) after domain 2 residues Gly130–Asp166 have been superimposed. (*b*) shows the LsrB–AI-2 complex from *Y. pestis* (yellow) and apo LsrB from *S. typhimurium* (red) after domain 2 residues Gly130–Asp166 have been superimposed. The locations of Gly130 and Asp166 are labelled and indicated by green spheres.

imposed on the domain 2 residues of the *S. typhimurium* LsrB–AI2 complex, the r.m.s.d. is 0.213 Å for the superimposed residues and 0.278 Å for the residues not included in the superposition, indicating there is very little (if any) difference in the tertiary structures of the two LsrB–AI-2 complexes. In contrast, an analogous superposition of the *Y. pestis* LsrB–AI-2 complex on *S. typhimurium* apo LsrB yields r.m.s.d.s of 0.274 and 2.525 Å for the superimposed and non-superimposed residues, respectively. This is indicative of a significant ligand-associated conformational change and explains why molecular replacement using the *S. typhimurium* apo LsrB structure failed to provide a solution for the *Y. pestis* LsrB–AI-2 complex.

3.2. AI-2 conformation and binding site

Strong electron density in the central cleft between the two α/β-domains was easily interpretable and was modelled as the *R*-THMF conformation of the AI-2 ligand (Fig. 3). These data are consistent with the *Y. pestis* LuxS and Pfs proteins synthesizing the non-boron-containing form of AI-2 and the *Y. pestis* LsrB recognizing this form of AI-2.

The AI-2 binding site in *Y. pestis* LsrB is highly conserved when compared with the binding sites of *S. typhimurium* and *Si. meliloti* LsrBs. The residues that form hydrogen bonds and van der Waals interactions with AI-2 are completely conserved in the three proteins (Fig. 1). Of particular note is the hydrogen bond between the C2 hydroxyl group of the AI-2 ring and the carbonyl O atom of Pro218 (Fig. 3), as this interaction, together with van der Waals interactions between the C2 methyl group and Phe40, Ala221, Leu264 and Trp265, may be necessary to differentially bind the 2*R* enantiomer over the 2*S* enantiomer. If AI-2 were to bind in the 2*S* conformation, both the carbonyl O atom of Pro218 and the C2 hydroxyl of AI-2 would be buried without hydrogen-bonding partners, a scenario that would be energetically unfavorable.

4. Conclusions

The structure of LsrB from *Y. pestis* complexed with autoinducer-2 (AI-2) has been solved by molecular replacement using the structure of LsrB from *S. typhimurium* (PDB entry 1tjy) and refined at 1.75 Å resolution. The electron density of the bound AI-2 matched the (2*R*,4*S*)-2-methyl-2,3,3,4-tetrahydroxytetrahydrofuran   (*R*-THMF)
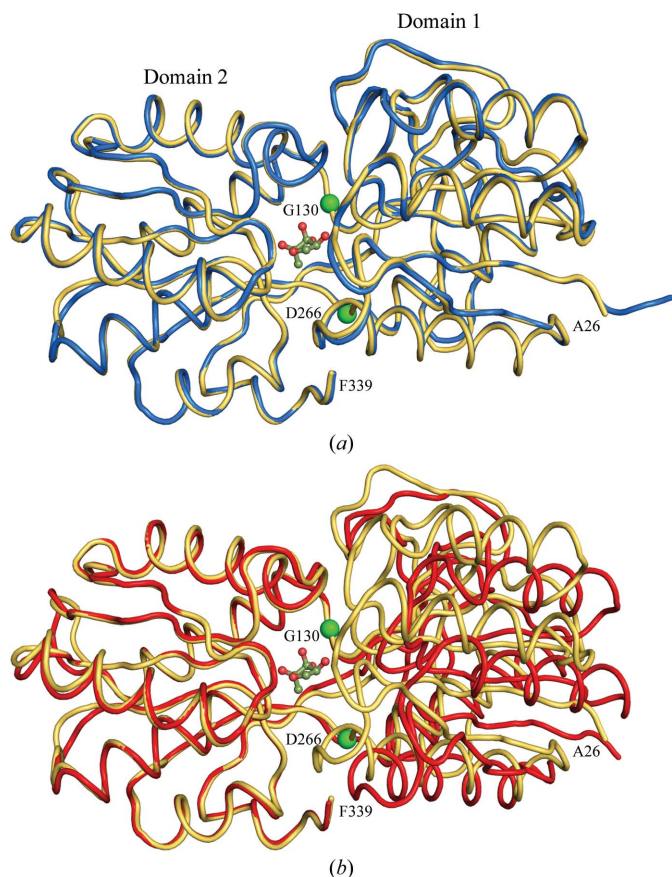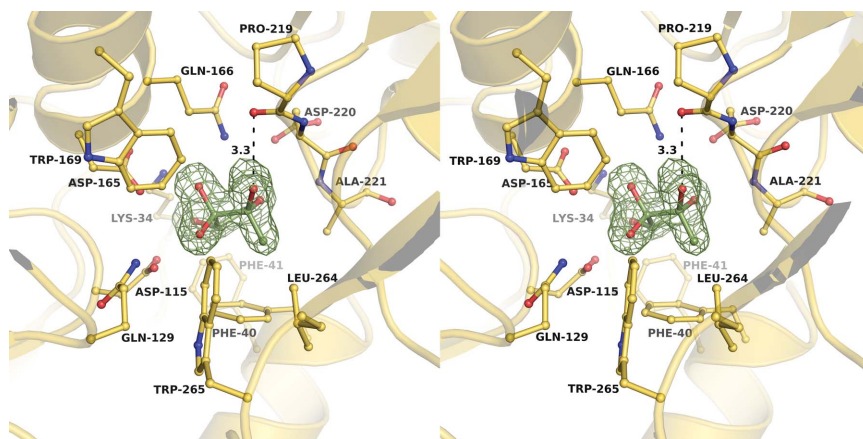

Figure 3
$F_o - F_c$ electron-density map calculated before the AI-2 molecule was added to the LsrB atomic model. Contours within 2.8 Å of the AI-2 molecule are drawn at 3σ. Residues that form hydrogen bonds or van der Waals interactions with the AI-2 molecule are shown as ball-and-stick models. The hydrogen bond between the C2 hydroxyl group of the AI-2 ring and the carbonyl O atom of Pro218 is indicated.

conformation, which is the same conformation that is bound by LsrBs from *S. typhimurium* and *Si. meliloti*.

References

Bassler, B. L., Wright, M., Showalter, R. E. & Silverman, M. R. (1993). *Mol. Microbiol.* **9**, 773–786.

Berman, H. M., Westbrook, J., Feng, Z., Gilliland, G., Bhat, T. N., Weissig, H., Shindyalov, I. N. & Bourne, P. E. (2000). *Nucleic Acids Res.* **28**, 235–242.

Bobrov, A. G., Bearden, S. W., Fetherston, J. D., Khweek, A. A., Parrish, K. D. & Perry, R. D. (2007). *Adv. Exp. Med. Biol.* **603**, 178–191.

Chen, X., Schauder, S., Potier, N., Van Dorsselaer, A., Pelczer, I., Bassler, B. L. & Hughson, F. M. (2002). *Nature (London)*, **415**, 545–549.

Dwyer, M. A. & Hellinga, H. W. (2004). *Curr. Opin. Struct. Biol.* **14**, 495–504.

Emsley, P., Lohkamp, B., Scott, W. G. & Cowtan, K. (2010). *Acta Cryst.* D**66**, 486–501.

Evans, P. (2006). *Acta Cryst.* D**62**, 72–82.

Fuqua, C., Parsek, M. R. & Greenberg, E. P. (2001). *Annu. Rev. Genet.* **35**, 439–468.

Gouet, P., Robert, X. & Courcelle, E. (2003). *Nucleic Acids Res.* **31**, 3320–3323.

Kabsch, W. (2010). *Acta Cryst.* D**66**, 125–132.

Larkin, M. A., Blackshields, G., Brown, N. P., Chenna, R., McGettigan, P. A., McWilliam, H., Valentin, F., Wallace, I. M., Wilm, A., Lopez, R., Thompson, J. D., Gibson, T. J. & Higgins, D. G. (2007). *Bioinformatics*, **23**, 2947–2948.

McCoy, A. J., Grosse-Kunstleve, R. W., Adams, P. D., Winn, M. D., Storoni, L. C. & Read, R. J. (2007). *J. Appl. Cryst.* **40**, 658–674.

Miller, S. T., Xavier, K. B., Campagna, S. R., Taga, M. E., Semmelhack, M. F., Bassler, B. L. & Hughson, F. M. (2004). *Mol. Cell*, **15**, 677–687.

Murshudov, G. N., Skubák, P., Lebedev, A. A., Pannu, N. S., Steiner, R. A., Nicholls, R. A., Winn, M. D., Long, F. & Vagin, A. A. (2011). *Acta Cryst.* D**67**, 355–367.

Pereira, C. S., McAuley, J. R., Taga, M. E., Xavier, K. B. & Miller, S. T. (2008). *Mol. Microbiol.* **70**, 1223–1235.

Quiocho, F. A. & Ledvina, P. S. (1996). *Mol. Microbiol.* **20**, 17–25.

Sun, J., Daniel, R., Wagner-Döbler, I. & Zeng, A.-P. (2004). *BMC Evol. Biol.* **4**, 36.

Surette, M. G., Miller, M. B. & Bassler, B. L. (1999). *Proc. Natl Acad. Sci. USA*, **96**, 1639–1644.

Taga, M. E., Miller, S. T. & Bassler, B. L. (2003). *Mol. Microbiol.* **50**, 1411–1427.

Taga, M. E., Semmelhack, J. L. & Bassler, B. L. (2001). *Mol. Microbiol.* **42**, 777–793.

Thoendel, M. & Horswill, A. R. (2010). *Adv. Appl. Microbiol.* **71**, 91–112.

Vendeville, A., Winzer, K., Heurlier, K., Tang, C. M. & Hardie, K. R. (2005). *Nature Rev. Microbiol.* **3**, 383–396.

Winn, M. D. et al. (2011). *Acta Cryst.* D**67**, 235–242.

Yu, J., Kavanaugh, J. S., Madsen, M. L., Carruthers, M. D., Phillips, G. J., Boyd, J. M., Horswill, A. R. & Minion, F. C. (2011). Submitted.